NANO LETTERS

pubs.acs.org/NanoLett Letter

Mitofusin-Decorated Extracellular Vesicles Enable Targeted Nucleic Acid Delivery to Mitochondria

Jiafeng Zhong, Luyao Wang,* Wenjing Xuan, Xuehan Xu, Xing Chang, Jianjun Cheng,* and Chengjie Sun*

Cite This: *Nano Lett.* 2026, 26, 6324−6333 Read Online

ACCESS | Metrics & More | Article Recommendations | Supporting Information

ABSTRACT: Mitochondria-targeted therapies hold great promise for treating metabolic syndrome, neurodegeneration, and cancers associated with mitochondrial dysfunction or genetic mutations. However, its advancement is significantly limited by the lack of effective and biocompatible targeted delivery systems. Here, we introduce mitofusin-decorated extracellular vesicles (MFNEVs) as a natural-sourced nanoplatform for efficient mitochondrial delivery of various cytoplasm-sensitive macromolecular cargos. The surface-displayed mitofusin proteins MFN1 and MFN2 direct MFNEVs to localize to mitochondria, as confirmed by confocal imaging and gel electrophoresis analysis. In both *in vitro* and *in vivo* models, siRNA-loaded MFNEVs effectively reduce the expression of mitochondrial DNA-encoded genes. Moreover, sgRNA-loaded MFNEVs can achieve CRISPR-based mitochondrial gene editing, resulting in a decreased mitochondrial DNA content. Mechanistic studies further reveal that the delivery is facilitated by the cooperation of the mitochondrial fusion machinery. These findings establish the feasibility and versatility of MFNEVs as a promising delivery solution for mitochondrial therapeutics.

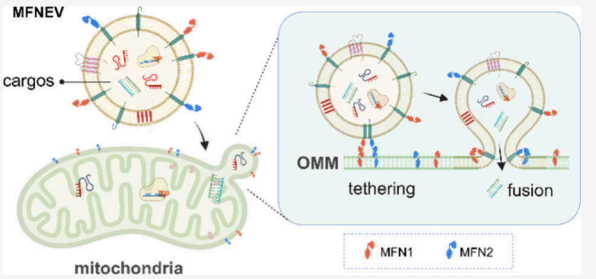

KEYWORDS: *mitochondria-targeted delivery, extracellular vesicles, mitofusin, siRNA, CRISPR*

Mitochondria play a pivotal role in cells, serving as the primary site for adenosine triphosphate (ATP) generation, the center for carbon and intermediate metabolism, and the critical signaling hub that determines cell function and fate.[1−4] Uniquely among organelles, they possess an autonomous genome encoding essential components of the oxidative phosphorylation machinery.[5] Consequently, mitochondrial dysfunction, especially genetic or epigenetic mutations within the mitochondrial genome, underlies numerous intractable disorders.[5−8] These include cancer, metabolic disease, neurodegeneration, aging, and most severely, mitochondrial genetic diseases for which only symptomatic treatments are available. These challenges have spurred growing interest in therapeutics that directly target mitochondria.[9,10]

However, unlike other cytoplasmic targets, the mitochondrial double membrane presents a formidable barrier to most drug molecules. This is particularly true for hydrophilic molecules and cytoplasm-sensitive macromolecules like nucleic acids. These limitations underscore the urgent need for efficient mitochondria-targeting delivery systems.[11,12] The key challenge is to establish effective interactions between mitochondria and the delivery vehicle or the cargo itself while keeping the integrity of mitochondrial structure and function.[13,14] In contrast, most of the conventional carriers such as liposomes and lipid nanoparticles undergo structural disassociation during the "endosome escape" process after cellular uptake to release the cargos,[15,16] which then lose the ability to cross the mitochondrial membrane barrier. Currently, there are mainly two strategies to achieve mitochondrial targeting: (i) covalent modification with lipophilic cations like triphenyl phosphonium (TPP^+) and cationic peptides.[13,14,17] This approach exploits the negative potential of the mitochondrial inner membrane to facilitate the accumulation of positively charged molecules. However, the enrichment of cations in mitochondria will decrease the membrane potential, inhibit mitochondrial respiration and trigger mitophagy due to the mitochondrial quality control mechanism,[14,18] making it less suitable for therapies aimed at restoring or improving mitochondrial function; and (ii) conjugation with mitochondria-targeting sequences (MTS),[19,20] which utilize the innate transport mechanism of nuclear-encoded mitochondrial proteins, but are largely limited to proteins or peptides. Overall, an efficient, biocompatible and versatile solution is still absent.

Received: January 15, 2026
Revised: May 6, 2026
Accepted: May 7, 2026
Published: May 11, 2026

https://doi.org/10.1021/acs.nanolett.6c00233
Nano Lett. 2026, 26, 6324−6333

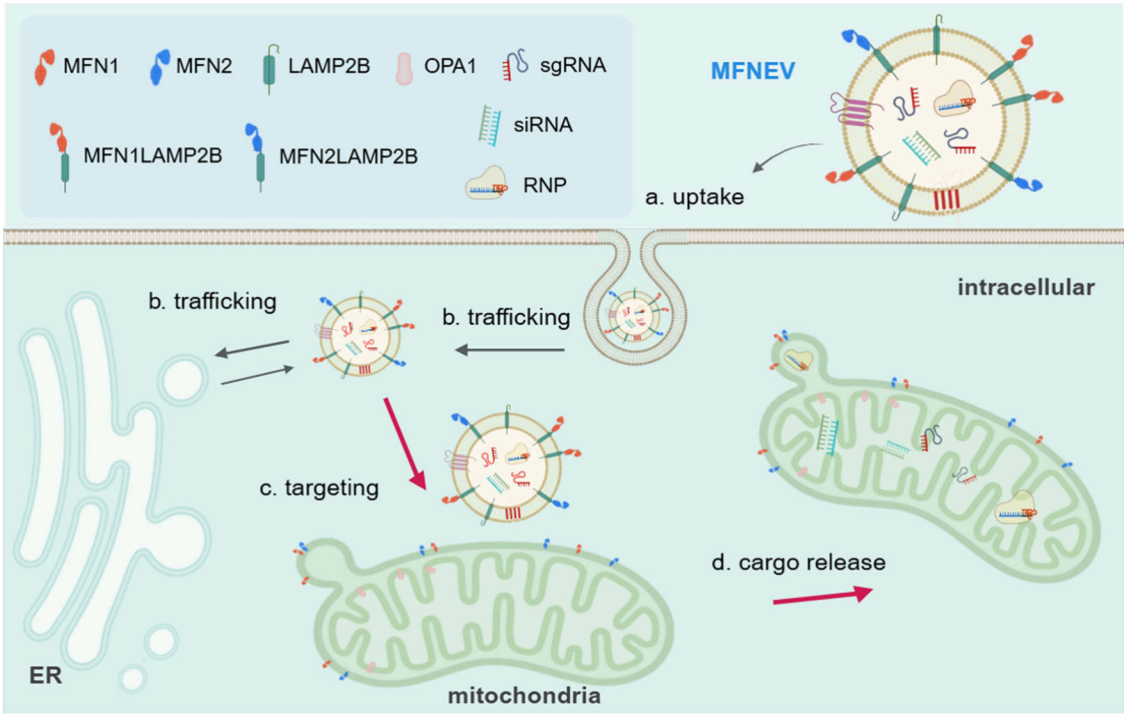

Figure 1. Schematic illustration of mitofusin-decorated extracellular vesicles (MFNEVs) for mitochondria-targeted nucleic acid delivery. MFNEVs are generated by functionalizing extracellular vesicles (EVs) with mitofusins through fusing MFN1 or MFN2 with the EV membrane protein LAMP2B. MFNEVs are (A) taken up by the recipient cells as intact vesicles and (B) sorted into the intracellular vesicle transport system. During the trafficking process, the MFN1 and MFN2 moieties on MFNEV (C) direct the vesicles toward mitochondria, leading to (D) mitochondrial association and cargo delivery.

Revisiting the intrinsic properties of mitochondria may offer new insights for the mitochondrial delivery of nonpermeable molecules. While the mitochondrial double membrane acts as a formidable barrier, it is also highly dynamic, undergoing continuous fusion and fission cycles that shape mitochondrial morphology and adapt to cellular demands.[11,12] These dynamic processes are mainly regulated by mitochondrial fusion and fission proteins: the dynamin-related protein 1 (DRP1) controls mitochondrial division,[21] whereas the mitofusins MFN1 and MFN2 mediate the outer membrane (OMM) fusion, and optic atrophy 1 (OPA1) predominantly drives the inner membrane (IMM) fusion between two mitochondria.[11,22−24] Beyond fission and fusion, the OMM forms contact sites with other organelles, including the endoplasmic reticulum (ER), lysosome, endosome, and the plasma membrane, to establish organelle communication and material exchange, which is mediated by the MFN2.[11,25] Moreover, mitochondria can secret small vesicles termed mitochondrial-derived vesicle (MDV), which exist in both single- and double-membraned forms. These MDVs shuttle selected cargoes to intracellular or extracellular space,[26,27] and can fuse with recipient mitochondria.[27,28]

Inspired from these, we developed a mitofusin-decorated extracellular vesicle (MFNEV) as a novel mitochondria-targeting delivery platform that harnesses the mitochondrial membrane dynamics. Extracellular vesicles (EVs) are cell-derived nanoparticles that participate in material transfer and intercellular communication.[29,30] Their inherent biocompatibility, physiological stability, high delivery efficiency, and engineerability render them attractive carriers for a wide range of therapeutics.[31−34] Unlike most nonviral vectors, EVs have been reported to enter the recipient cells as intact vesicles and surf among the intracellular vesicle trafficking circuits.[35,36] Here, we displayed mitofusins MFN1 and MFN2 on the EV surface to generate MFNEVs. These vesicles are designed to engage mitochondrial MFN1 and MFN2 through the formation of mitofusin homomultimers and heteromultimers. Such interactions promote the vesicle-mitochondrion tethering, potentially followed by membrane fusion. This process is proposed to enable mitochondria-targeted cargo delivery (Figure 1). In proof-of-concept experiments, we show that siRNA-loaded MFNEVs efficiently locate to mitochondria, enabling targeted siRNA accumulation in mitochondria. In both *in vitro* and *in vivo* models, siRNA-loaded MFNEVs significantly reduced mitochondrial encoded gene expression at the mRNA level. More importantly, sgRNA-packaged MFNEVs enabled CRISPR-mediated mitochondrial DNA editing. These results established MFNEVs as a potent and versatile delivery platform for mitochondria-targeted therapy.

PREPARATION AND CHARACTERIZATION OF MFNEVs

To generate MFNEVs, mitofusins MFN1 and MFN2 were fused to the extra-vesicular N terminus of human LAMP2B, a membrane protein widely used for EV surface engineering[31,37] (Figure 2A, Figure S1 and Figure S2). The MFN1 or MFN2 fragment was cloned into the region between the signal peptide and the transmembrane domain of LAMP2B, and the resulting plasmids were sequence-verified. Lentiviral vectors encoding the two fusion proteins were produced and transduced into HEK 293T cells. The MFN1-LAMP2B/MFN2-LAMP2B double positive clone of HEK 293T cell was obtained by single-cell sorting and puromycin/hygromycin selection. The cell clones were confirmed by PCR amplification of the fused

https://doi.org/10.1021/acs.nanolett.6c00233
Nano Lett. 2026, 26, 6324−6333

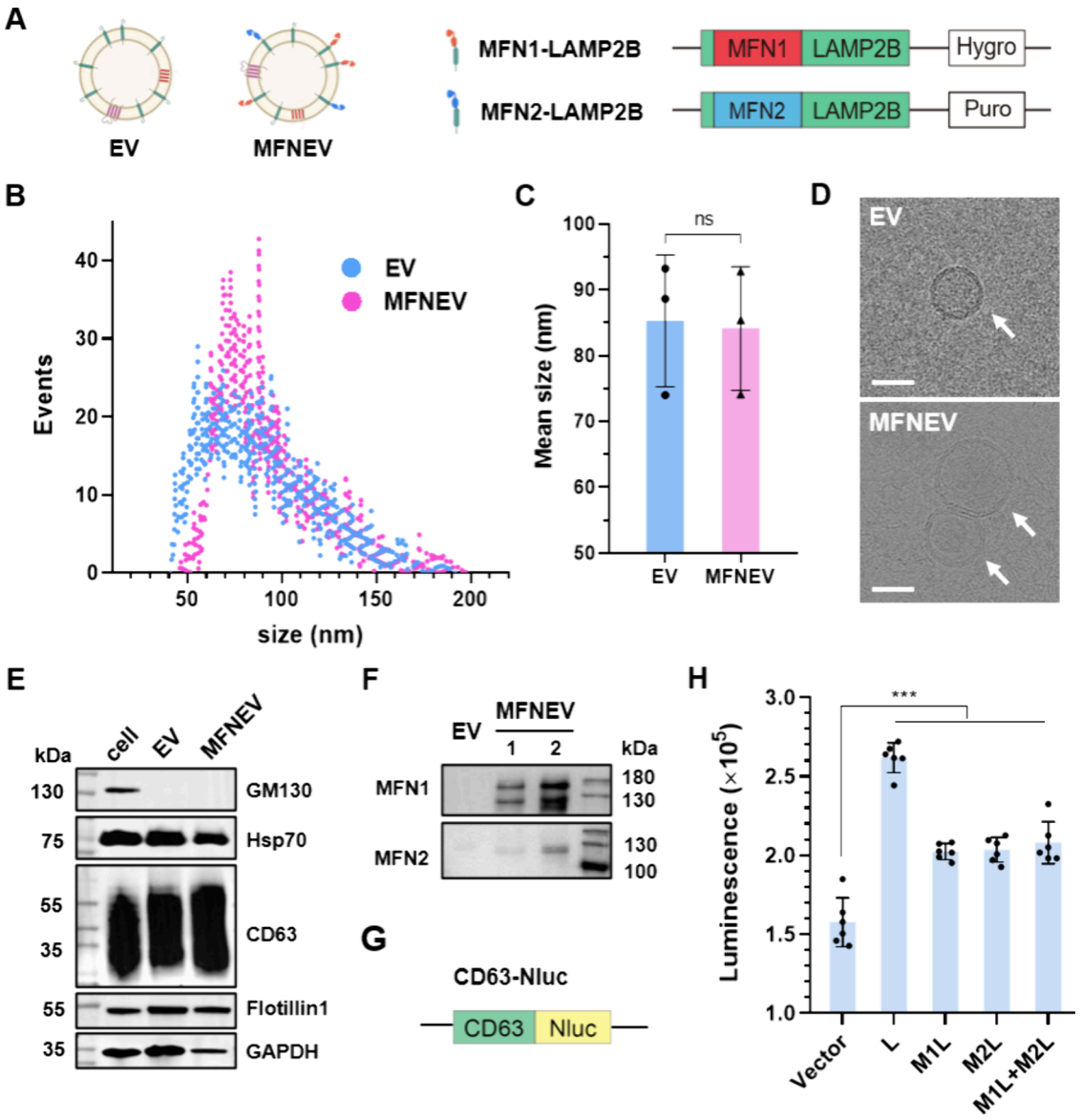

Figure 2. Characterization of MFNEVs. (A) Schematic illustration of EV and MFNEV, and the construction of MFN1-LAMP2B and MFN2-LAMP2B fusion proteins. MFN1 or MFN2 was cloned into the downstream of the LAMP2B signal sequence. (B) Particle size distribution of EVs and MFNEVs analyzed using a Flow NanoAnalyzer. (C) Mean diameters of MFNEVs and EVs calculated from three independent batches (mean ± SD $n = 3$; Student's t-test). (D) Typical cryo-EM images of EVs and MFNEVs. Scale bars, 50 nm. (E) Biomarkers of EVs and MFNEVs analyzed by Western blotting. (F) Immunoblotting of MFN1-LAMP2B and MFN2-LAMP2B expression on EVs and MFNEVs using anti-MFN1 and anti-MFN2 antibodies. MFNEVs derived from two different clones of parent cells are denoted as "1" and "2". (G) Construction of the CD63-Nluc plasmid. The nanoluciferase was fused to the C terminus of the vesicular membrane protein CD63. (H) The influence of MFN1-LAMP2B and MFN2-LAMP2B expression on extracellular vesicle secretion. HEK 293T-CD63-Nluc cells were transfected with the indicated plasmids and the supernatants were collected after 48 h for bioluminescence as a readout of vesicular secretion. L, LAMP2B; M1L, MFN1-LAMP2B; M2L, MFN2-LAMP2B. Statistical significance was calculated by one-way ANOVA using the Vector group as control (mean ± SD $n = 6$). ***$P < 0.001$; ns, not significant.

region (Figure S3). MFNEVs were purified from the supernatants of the culture medium by PEG precipitation combined with size exclusion chromatography (SEC) method to improve purity and minimize irreversible aggregation.[38] Flow NanoAnalyzer measurements[39] showed particle diameters ranging from 40 to 200 nm (mean ∼ 85 nm), with no significant difference compared to normal EVs (Figure 2B,C). In addition, MFNEVs exhibited a representative vesicular morphology under cryo-EM (Figure 2D). Immunoblotting of MFNEVs showed typical EV-specific markers CD63, HSP70 and Flotillin1, but not the Golgi apparatus-associated protein GM130, as well as the fusion proteins MFN1-LAMP2B and MFN2-LAMP2B (∼130 kDa), demonstrating the successful decoration of MFN1 and MFN2 (Figure 2E,F).

To further characterize MFNEVs, we stained MFNEVs from independent batches with anti-MFN1 and anti-MFN2 antibodies and analyzed them using the Flow NanoAnalyzer. The results showed that 91.3 ± 2.5% of the MFNEVs were MFN1 positive, and 82.0 ± 2.7% were MFN2 positive (Figure S4), supporting surface accessibility of MFN1/MFN2 epitopes on MFNEVs surface. To assess the influence of expression of MFN1-LAMP2B and MFN2-LAMP2B on the extracellular

https://doi.org/10.1021/acs.nanolett.6c00233
Nano Lett. 2026, 26, 6324−6333

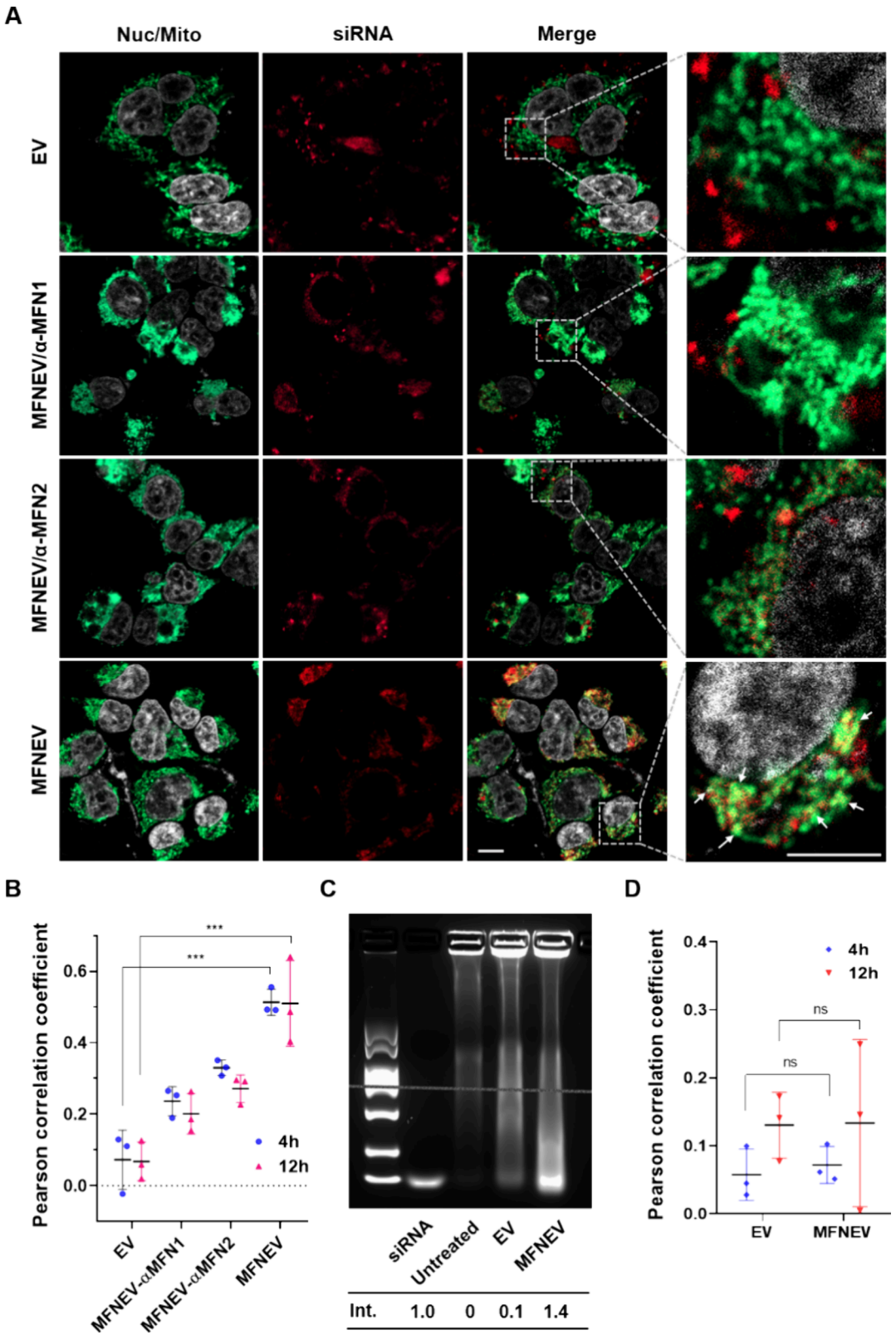

Figure 3. MFNEVs efficiently target mitochondria. (A) Confocal fluorescence microscopy images of HEK 293T-mitoEGFP cells after 4 h incubation with EVs or MFNEVs. Cy5-labeled siRNA (red) was loaded into EVs and MFNEVs for intracellular vesicle tracking. For MFNEV/α-MFN1 and MFNEV/α-MFN2 experiments, MFNEVs were preincubated with anti-MFN1 and anti-MFN2 antibodies before cell treatment, respectively. The cells were stained with NucBlue (gray) for nucleus visualization. Mitochondria expressing mitoEGFP are indicated by Mito (green). White arrows point to typical colocalization of siRNA with mitochondria. Scale bars, 10 μm. (B) Pearson correlation coefficients quantifying the colocalization of Cy5-siRNA and mitochondrial signals at 4 and 12 h, calculated using ZEN software from three distinct fields. Data are presented as mean ± SD (n = 3), and Student's t-test was applied. ***P < 0.001. (C) Gel electrophoresis image of isolated mitochondria samples. Mitochondria were isolated from HEK 293T cells treated with or without siRNA-loaded EVs or MFNEVs, digested with proteinase K, and

https://doi.org/10.1021/acs.nanolett.6c00233
Nano Lett. 2026, 26, 6324−6333

Figure 3. continued

subjected to a 2% agarose gel. Twenty-five ng of free siRNAs were loaded as a control. Relative band intensities (Int.) were quantified using ImageJ software. (D) Pearson correlation coefficients quantifying the colocalization of Cy5-siRNA with lysosome at 4 and 12 h, calculated using ZEN software from three distinct fields. Data are presented as mean ± SD (n = 3), and Student's t-test was applied. ns, not significant.

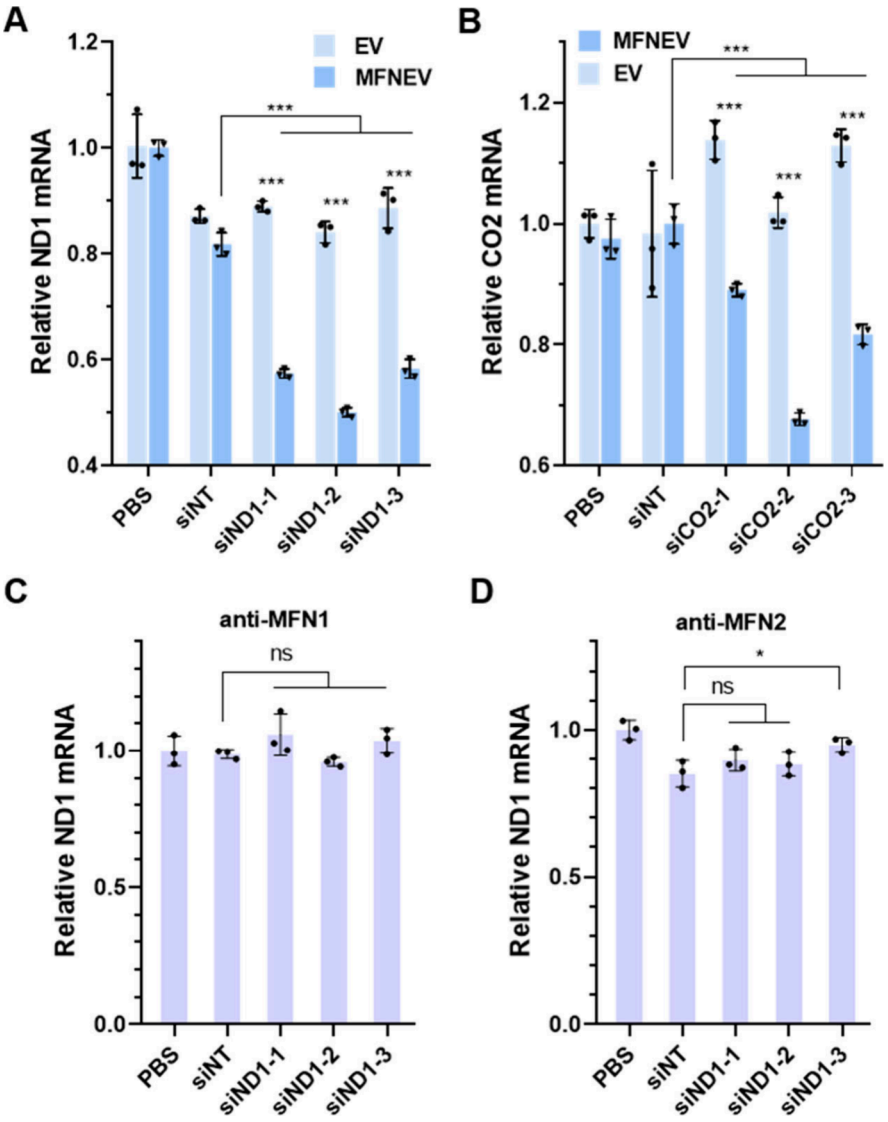

Figure 4. *In vitro* mitochondrial siRNA delivery. (A) Relative ND1 mRNA levels in HEK 293T cells treated with MFNEVs or EVs (5 pmol siND1 per 4 × 10^5 cells). (B) Relative CO_2 mRNA levels in HEK 293T cells treated with MFNEVs or EVs (5 pmol siCO2 per 4 × 10^5 cells). (C, D) Relative ND1 mRNA levels in cells treated with siND1-loaded MFNEVs preincubated with (C) anti-MFN1 or (D) anti-MFN2 antibodies. HEK 293T cells were incubated with siRNA-loaded EVs or MFNEVs for 24 h (three distinct siRNA sequences per target). Total mRNA was isolated for qPCR analysis, using mitochondrial 16s rRNA as an internal reference. Data are presented as mean ± SD (n = 3). Statistical significance was determined by one-way ANOVA (a, b, d, e, f) and multiple t-tests (b, d). *P < 0.05; ***P < 0.001; ns, not significant.

vesicle secretion, we generated a HEK 293T CD63-Nluc cell line via lentiviral transduction to quantify EV release by bioluminescence (Figure 2G and Table S3). Compared to the empty plasmid vector, transient transfection with LAMP2B alone led to a significant increase (>65%) in EV secretion after 24 h. However, the fusion of either MFN1 or MFN2 with LAMP2B attenuated this enhancing effect, but still remained ~30% higher (Figure 2H), suggesting a boosted vesicle production in MFN1-LAMP2B/MFN2-LAMP2B double positive HEK 293T cells. Finally, MFNEVs showed no apparent effect on recipient cell proliferation (Figure S5), mitochondrial morphology (Figure S6), ATP production (Figure S7), or mitochondrial membrane potential (Figure S8) across the tested dose range, providing strong support for the biocompatibility of MFNEVs.

MITOCHONDRIAL-TARGETING ABILITY OF MFNEVs

To demonstrate the mitochondrial-targeting capability of MFNEV, we packaged MFNEVs with Cy5-labeled siRNA (Table S2, Figure S9) via electroporation for intracellular tracing. After loading, MFNEVs retained characteristic vesicular morphology (Figure S10), and no significant changes

https://doi.org/10.1021/acs.nanolett.6c00233
Nano Lett. 2026, 26, 6324−6333

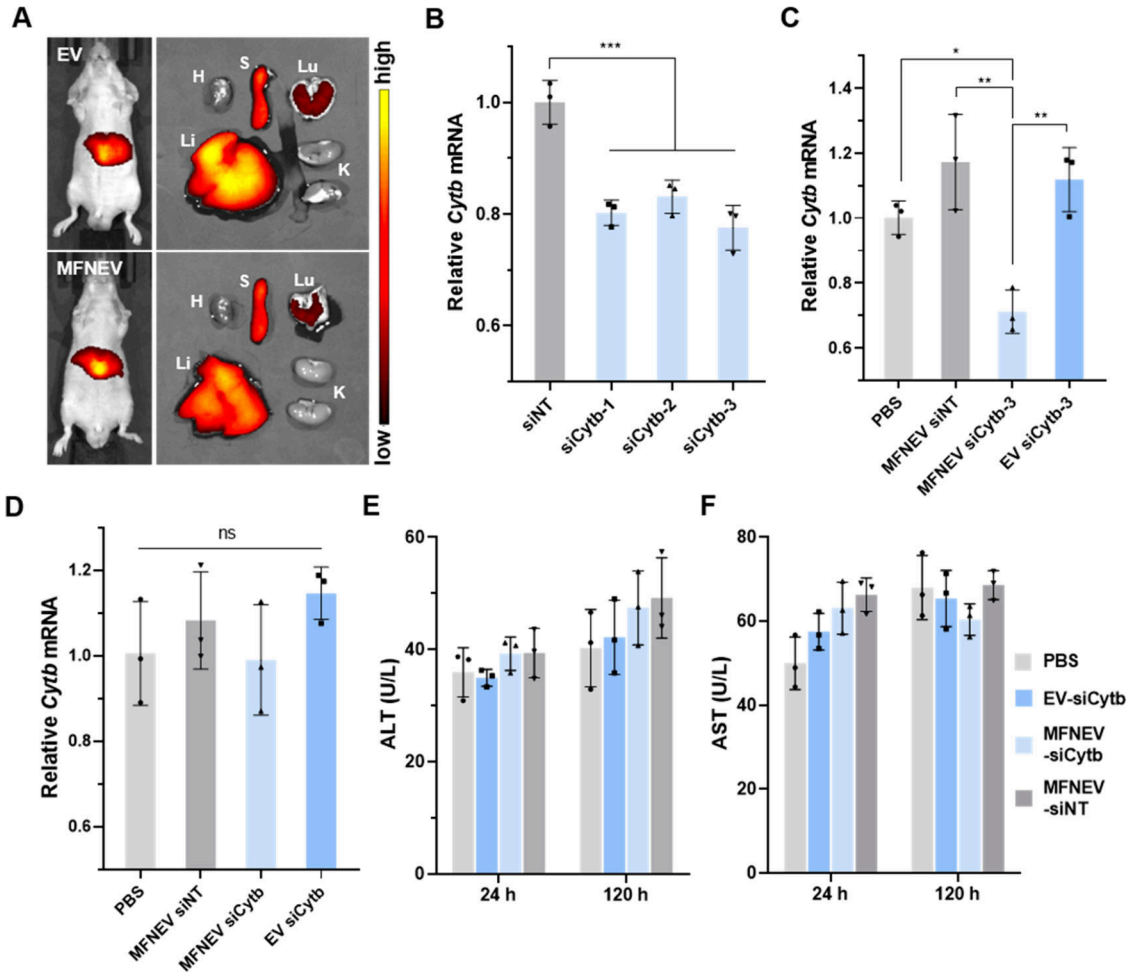

Figure 5. *In vivo* mitochondrial siRNA delivery. (A) Distribution of siCy5-loaded EVs and MFNEVs in mice (left) and in excised organs (right). H, heart; Li, liver; S, spleen; Lu, lung; K, kidney. (B to D) Relative *Cytb* mRNA levels in liver tissues of mice following different siRNA treatments: (B) 2 μg siRNA per 20 g body weight delivered via MFNEVs; (C, D) 4 μg siRNA per 20 g body weight delivered via MFNEVs or EVs. siCytb-1, -2, and -3 represent distinct sequences of *Cytb* siRNA. (E) Serum ALT and (F) AST levels in mice after the administration of siRNA-loaded EVs or MFNEVs. Data are presented as mean ± SD (n = 3). Statistical significance was determined by one-way ANOVA. *P < 0.05; **P < 0.01; ***P < 0.001; ns, not significant.

in particle size distribution were observed (Figure S11), supporting preservation of vesicle structure. A mitoGFP (mitochondrial targeting sequence of COX8 fused to the N terminus of GFP) was stably transduced into HEK 293T cells to serve as an indicator of the mitochondrial matrix. Cells (4×10^5) were treated with 40 μg of EVs or MFNEVs (containing ~0.5 μg siRNA), and fluorescence images were captured using laser scanning confocal microscopy (LSCM). In the MFNEV group, numerous yellow dots were observed at both 4 and 12 h post-treatment (Figure 3A and Figure S12), indicating strong spatial overlap between the Cy5-siRNA signal (red) and mitoGFP-labeled mitochondrial regions (green). In contrast, colocalization was minimal in cells treated with unmodified EVs, as further confirmed by multimodality structured illumination microscopy (Multi-SIM) imaging of both living cells (Figure S13) and isolated mitochondria (Figure S14). Pearson correlation analysis across three independent fields confirmed a strong colocalization of siRNA with mitochondria in MFNEV-treated cells relative to EV controls (~0.51 versus ~0.07 at 4 h, Figure 3B). To probe the interaction between MFNEVs and mitochondria, we performed a lipid diffusion assay using DiI-labeled vesicles (Figure S15). In MFNEV-treated cells, the DiI signal was observed to closely associate with mitochondrial structures, whereas no such behavior was observed for unmodified EVs, supporting MFN-dependent membrane interaction and lipid exchange. In the meanwhile, blocking either MFN1 or MFN2 with the helix bundle domain-binding antibodies significantly reduced colocalization (~0.23 and ~0.32, respectively, Figure 3A,B), and this antibody treatment did not measurably affect cellular uptake (Figure S16), consistent with the established membrane fusion-driving roles of both mitofusins for mitochondrial fusion.[11,22] To further confirm the mitochondrial delivery, mitochondria were isolated from the HEK 293T cells 24 h after treatment with Cy5-siRNA-loaded EVs or MFNEVs. The purified mitochondria were then digested with proteinase K and analyzed by agarose gel electrophoresis (Figure 3C). Purified mitochondria were also sequentially treated with digitonin and RNase before proteinase K digestion and gel analysis (Figure S17). In both assays, a clear siRNA band was detected in the MFNEV group, supporting efficient intramitochondrial delivery. In contrast, no obvious siRNA band was observed in the EV group, underscoring the indispensable role of mitofusin decoration for mitochondrial delivery. Additionally, lysosomal localization was also assessed using LysoTracker staining. Minimal overlap between lysosomes and Cy5-siRNA was observed in either EV-

https://doi.org/10.1021/acs.nanolett.6c00233
Nano Lett. 2026, 26, 6324−6333

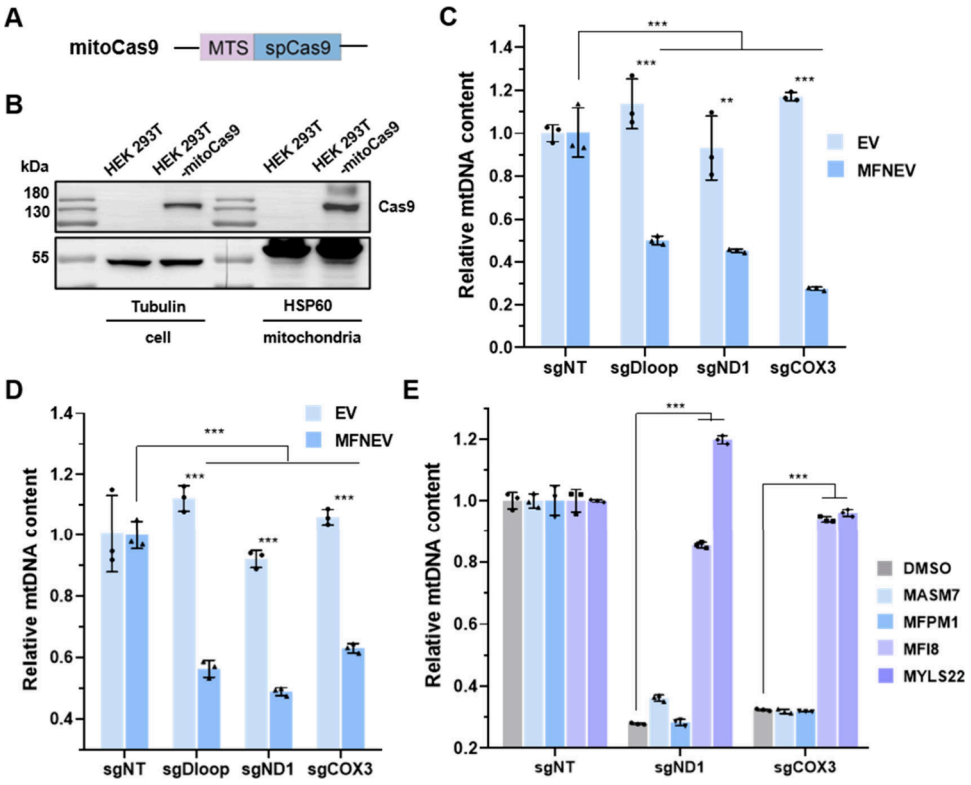

Figure 6. Mitochondrial DNA editing by CRISPR-Cas9. (A) Construction of mitochondrial Cas9 (mitoCas9). The mitochondrial targeting sequence (MTS) of COX8 protein was fused to the N terminus of spCas9. (B) Immunoblotting of Cas9 expression in whole-cell and mitochondrial fractions from HEK 293T or HEK 293T-mitoCas9 cells. (C) Relative mtDNA content in HEK 293T-mitoCas9 cells 16 h after treatment with either MFNEV-sgRNA or EV-sgRNA, detected by qPCR and normalized to the sgGFP group. (D) Relative mtDNA content in HEK 293T cells treated with either MFNEV-RNP or EV-RNP. (E) Relative mtDNA content in HEK 293T-mitoCas9 cells pretreated for 2 h with mitochondrial fusion inhibitors (MFI8, 20 μM; MYLS22, 30 μM) or post-treated for 2 h with mitochondrial fusion promotors (MASM7, 1 μM; MFPM1, 20 μM), followed by incubation with the indicated MFNEV-sgRNA. mtDNA content was analyzed by qPCR 16 h later. Data are presented as mean ± SD (n = 3). Statistical significance was determined by one-way ANOVA and multiple t-tests. $^{**}P < 0.01$; $^{***}P < 0.001$.

or MFNEV-treated cells at all time points (Figure S18), as reflected by low Pearson correlation coefficients (Figure 3D), indicating the negligible lysosomal sequestration.

IN VITRO AND *IN VIVO* siRNA DELIVERY TO MITOCHONDRIA VIA MFNEV

In mammalian cells, the mitochondrial RNA import machinery is generally considered absent, limiting the application of RNA interference (RNAi) for mitochondrial genome regulation in both fundamental research and therapeutic context, although RNAi-like mechanism in mitochondria has been reported.[40,41] Having confirmed the mitochondrial targeting capability of MFNEVs, we next examined whether the delivered siRNA could function within mitochondria. siRNAs against the mitochondrial DNA (mtDNA)-encoded ND1 and COX2 genes (siND1 and siCO2; Table S2) were packaged into MFNEVs by electroporation. The obtained siND1-loaded MFNEVs and siCO2-loaded MFNEVs were then separately incubated with HEK 293T cells. Relative mRNA expression levels were quantified by RT-qPCR using mtDNA-encoded 16S rRNA as internal control.[40] Cells treated with empty MFNEVs were also analyzed to exclude the influence of MFN1-LAMP2B and MFN2-LAMP2B on ND1 and COX2 mRNA expression (Figure S19A). Unexpectedly, a siRNA dose typically used for nuclear DNA-encoded targets (30 pmol per 4 × 10^5 cells) caused a dramatic increase in ND1 mRNA expression at 24 h post-treatment compared with the negative control (Figure S20A), while a lower dose (5 pmol per 4 × 10^5 cells) reduced ND1 mRNA by more than 40% (Figure 4A). In contrast, the mRNA level of the nontargeted mtDNA-encoded gene ATP6 was not affected (Figure S21). The downregulation was further confirmed by Western blot, which showed a significant reduction of ND1 protein at 48 h (Figure S20B). Treatment of HEK 293T cells with siCO2-loaded MFNEVs also led to a mild reduction of CO2 mRNA (~20%−30%, Figure 4B). Moreover, MFNEVs similarly decreased ND1 mRNA in HeLa cells (Figure S19B), demonstrating cross-cell-line applicability, albeit with reduced delivery efficiency. To exclude potential confounding effects arising from fluctuations in mtDNA abundance, ND1 transcript levels were additionally normalized to a nuclear-encoded reference gene (SDHA). Consistent with the initial analysis, ND1 expression remained significantly reduced under this normalization scheme (Figure S22). Notably, the decline of ND1 mRNA was completely abolished when either MFN1 or MFN2 on the MFNEVs was blocked by antibodies before cell incubation (Figure 4C,D), consistent with the colocalization data (Figure 3A). Collectively, these results strongly demonstrate that MFNEVs can efficiently deliver siRNAs to mitochondria and modulate mtDNA-encoded gene expression.

Given the high sequence conservation of MFN1 (96.1%) and MFN2 (98.8%) between human and mouse (analyzed by SanpGene), we next validated MFNEV-mediated mitochondria-targeting siRNA delivery *in vivo*. EVs or MFNEVs loaded

https://doi.org/10.1021/acs.nanolett.6c00233
Nano Lett. 2026, 26, 6324−6333

with Cy5-labeled siRNA were systemically administrated into BALB/c-Nude mice to evaluate their biodistribution. In both groups, Cy5 signals were predominantly localized to the liver tissue (Figure 5A), indicating that mitofusin decoration had minimal impact on organ biodistribution. To study the capability of MFNEVs for *in vivo* applications, siRNAs targeting the mouse mitochondria DNA encoded cytochrome *b* (*Cytb*) (Table S2) were loaded into MFNEVs and injected intravenously at 2 μg or 4 μg per 20 g body weight. Total RNA was extracted from the liver tissue and qPCR analysis was applied to determine the mRNA levels. Screening of three siRNA sequences (siCytb-1-3, Table S2) revealed that all these sequences effectively reduced *Cytb* at mRNA levels (Figure 5B), and siCytb-3 was used for subsequent studies. At 24 h postinjection, siCytb-3-loaded MFNEVs reduced *Cytb* mRNA by ~30%, indicating the successful downregulation of mtDNA expression via siRNA delivery *in vivo*. In contrast, the mRNA level remained unchanged in the EV group (Figure 5C), implying that MFN1 and MFN2 are essential for mitochondrial targeting and siRNA release. Moreover, Cytb transcript levels were significantly reduced in the mitochondrial fraction of the MFNEV-treated group, whereas no reduction was observed in the EV-siCytb control group (Figure S23). These results provide compartment-specific evidence supporting mitochondrial delivery of siRNA *in vivo*. The mRNA levels returned to normal levels by 120 h post-treatment (Figure 5D). Additionally, the blood biochemical indicators alanine aminotransferase (ALT) and aspartate aminotransferase (AST) remained in low levels (Figure 5E,F), confirming the biocompatibility of MFNEVs. These results demonstrate that the MFNEV system is highly capable of *in vivo* mitochondria-targeted siRNA delivery with a strong safety profile.

MFNEV ENABLES CRISPR-MEDIATED GENE EDITING IN MITOCHONDRIA

While programmable CRISPR-Cas (clustered regularly interspaced short palindromic repeats associated with a Cas endonuclease)-based technologies have revolutionized nuclear genome editing, their application to mitochondrial DNA has remained restricted to gRNA delivery. This is primarily due to the lack of entries for importing DNA or RNA strands into mammalian mitochondria.[42,43] Benefiting from the versatility of extracellular vesicles for encapsulating various types of cargos,[29,33] we explored the potential of MFNEVs to deliver single-guide RNA (sgRNA), which is essential for the Cas nuclease activity. To test this, we fused the mitochondrial targeting sequence (MTS) of COX8 to the N terminus of the Cas9 (mitoCas9, Figure 6A, Table S3) and generated a HEK 293T cell line stably expressing this fusion protein through lentivirus transduction (HEK 293T mitoCas9, Figure 6B, Figure S24). Four sgRNAs were designed to target the mitochondrial D-loop region (sgDloop), the NADH dehydrogenase subunit 1 (sgND1), the cytochrome c oxidase subunit 3 (sgCO3), and green fluorescent protein (sgGFP, as negative control) (Table S2). These sgRNAs were delivered into the HEK 293T-mitoCas9 cells using either MFNEVs or EVs. Since linearized mtDNA is rapidly degraded by the exonuclease instead of repairing through homologous recombination (HR) or nonhomologous end-joining (NHEJ) exonucleolytic activities in mitochondria,[44−46] the Cas9-induced double-strand break will lead to a decrease of mtDNA copy number, which can be quantified by qPCR. Strikingly, treatment with 0.5 μg of sgRNA per 4 × 10^5 of HEK 293T-mitoCas9 cells induced a significant decrease in mtDNA content in the MFNEV group at 16 h, with a maximum reduction of 70% relative to the sgGFP control (Figure 6C). To further assess whether the observed effects arise from generalized mitochondrial loss, we evaluated the expression of the mitochondrial matrix protein HSP60. Immunoblot analysis showed that HSP60 levels remained stable across all treatment groups (Figure S25), consistent with the absence of global mitochondrial degradation. Notably, no obvious change in mitochondrial abundance was observed by microscopy (Figure S26). Meanwhile, the mtDNA content remained unchanged when the same amount of sgRNA was delivered by EVs. Furthermore, when Cas9 protein-sgRNA complexes (RNP, Figures S10 and S27) were directedly packaged into EVs or MFNEVs and applied to the HEK 293T cells, mtDNA reduction was again observed only in the MFNEV group (Figure 6D). Notably, pretreatment of MFNEVs with anti-MFN1 or anti-MFN2 antibodies eliminated the delivery outcome (Figure S28), further supporting mitofusin-dependent delivery. These results demonstrate that MFNEVs present a promising delivery solution for expanding the application of CRISPR-based tool kit in mitochondrial gene editing.

MFNEV DELIVERY RELIES ON THE MITOCHONDRIAL FUSION MACHINERY

We next examined how regulation of mitochondrial membrane fusion affects the MFNEV delivery efficiency, as our system was designed to hijack the mitochondrial fusion machinery. We hypothesized that promoting mitochondrial fusion would enhance MFNEV-mitochondria fusion and enable broader cargo distribution throughout the mitochondrial network, thereby improving the delivery outcomes. Conversely, inhibiting mitochondrial fusion would block the MFNEV delivery. Unexpectedly, supplementation with the mitochondrial fusion agonists MFP M1[47] (20 μM) or MASM7[48] (1 μM) did not further decrease the relative mtDNA content compared to the solvent control (Figure 6E). While inhibition of mitochondrial fusion—either with the specifically outer membrane fusion inhibitor MFI8[48] (20 μM) or the inner membrane fusion inhibitor MYLS22[49] (30 μM) treatment—completely prevented the sgRNA-induced reduction in mtDNA level (Figure 6E). To further assess the role of mitochondrial fusion machinery at genetic level, we performed siRNA-mediated knockdown of MFN1 and OPA1. Efficient depletion was confirmed at the protein level by immunoblotting (Figures S29A and S30A). Under these conditions, the delivery efficiency of MFNEV-sgND1, as measured by changes in relative mtDNA content, was markedly reduced compared to control cells (Figures S29B and S30B). These findings support the view that MFNEV-mediated cargo delivery is consistent with a working model involving the mitochondrial fusion machinery.

In conclusion, we developed a mitofusin-decorated extracellular vesicle (MFNEV) system for effective and biocompatible mitochondria-targeted delivery. Distinguished from conventional membrane potential-driven targeting strategies, MFNEV naturally employs the intrinsic mitochondrial fusion machinery for delivery without disturbing mitochondrial functions under the experimental conditions tested. With siRNA-loaded MFNEVs, we achieved efficient and low-toxicity downregulation of mtDNA expression in both *in vitro* and *in vivo* models. Moreover, CRISPR-based mtDNA editing was successfully executed through sgRNA delivery with MFNEVs.

https://doi.org/10.1021/acs.nanolett.6c00233
Nano Lett. 2026, 26, 6324−6333

These findings establish MFNEVs as a promising and versatile platform for mitochondria-targeted delivery. We anticipate that our MFNEV technique, combined with the high engineerability of extracellular vesicles, will significantly benefit future research and therapeutic development in mitochondria-related fields.

■ ASSOCIATED CONTENT

Data Availability Statement

All data supporting the findings of this study are available within the paper and its Supporting Information.

Supporting Information

The Supporting Information is available free of charge at https://pubs.acs.org/doi/10.1021/acs.nanolett.6c00233.

Additional experimental materials and methods, tables for primer, siRNA, and sgRNA sequences, plasmid maps and cell line validation, MFNEV physical characterization including cryo-EM and Flow NanoAnalyzer data, mitochondrial toxicity and biosafety evaluations, cargo loading efficiency, high-resolution Multi-SIM imaging and colocalization analysis, RNase and protease protection assays, CRISPR/Cas9 editing validation (PDF)

■ AUTHOR INFORMATION

Corresponding Authors

Luyao Wang − *Department of Materials Science and Engineering, Westlake University, Hangzhou, Zhejiang 310030, China*; Email: wangluyao@westlake.edu.cn

Jianjun Cheng − *Department of Materials Science and Engineering and Research Center for Industries of the Future, Westlake University, Hangzhou, Zhejiang 310030, China; Institute of Advanced Technology, Westlake Institute for Advanced Study, Hangzhou, Zhejiang 310024, China;* orcid.org/0000-0003-2561-9291; Email: chengjianjun@westlake.edu.cn

Chengjie Sun − *Department of Materials Science and Engineering, Westlake University, Hangzhou, Zhejiang 310030, China;* orcid.org/0000-0001-6038-1616; Email: sunchengjie@westlake.edu.cn

Authors

Jiafeng Zhong − *Fudan University, Shanghai 200433, China; School of Medicine, Westlake University, Hangzhou, Zhejiang 310023, China*

Wenjing Xuan − *Department of Materials Science and Engineering, Westlake University, Hangzhou, Zhejiang 310030, China*

Xuehan Xu − *Department of Materials Science and Engineering, Westlake University, Hangzhou, Zhejiang 310030, China*

Xing Chang − *School of Medicine, Westlake University, Hangzhou, Zhejiang 310023, China*

Complete contact information is available at: https://pubs.acs.org/10.1021/acs.nanolett.6c00233

Author Contributions

J.Z., C.S., and J.C. conceived the ideas and designed the experiments. J.Z. performed the experiments and data analysis and wrote the manuscript. X.X., L.W., and W.X. contributed reagents, materials, and analysis tools and provided suggestions for methodology. W.X., C.S., X.C., and J.C. provided suggestions for manuscript writing. C.S., L.W., and J.C. were responsible for funding acquisition and supervision.

Notes

The authors declare the following competing financial interest(s): J.Z., C.S., and J.C. are inventors on a preparing patent application related to this work by Westlake University. The authors declare that they have no other competing interests.

■ ACKNOWLEDGMENTS

This work was supported by the "Pioneer" and "Leading Goose" R&D Program of Zhejiang (2024SDXHDX0004), the National Natural Science Foundation of China 52203187 (C.S.) and 52233015 (J.C.), and the Zhejiang Province Postdoctoral Research Project Selective Support (ZJ2025026, L.W.). We acknowledge the support of the New Cornerstone Investigator Program and the New Cornerstone Science Foundation. We acknowledge the support from the Laboratory Animal Resources Center, the Biomedical Research Core Facilities, and the Instrumentation and Service Center for Physical Sciences in Westlake University. We thank the Microscopy Core Facility of Westlake University for the facility support and also thank technician Fang Xiao for the help of taking and analyzing Multi-SIM images.

■ REFERENCES

(1) Disha, B.; Mathew, R. P.; Dalal, A. B.; Mahato, A. K.; Satyamoorthy, K.; Singh, K. K.; Thangaraj, K.; Govindaraj, P. Mitochondria in biology and medicine-2023. *Mitochondrion* **2024**, *76*, No. 101853.

(2) Harrington, J. S.; Ryter, S. W.; Plataki, M.; Price, D. R.; Choi, A. M. K. Mitochondria in health, disease, and aging. *Physiol. Rev.* **2023**, *103* (4), 2349−2422.

(3) Nunnari, J.; Suomalainen, A. Mitochondria: In sickness and in health. *Cell* **2012**, *148* (6), 1145−1159.

(4) Monzel, A. S.; Enriquez, J. A.; Picard, M. Multifaceted mitochondria: Moving mitochondrial science beyond function and dysfunction. *Nat. Metab.* **2023**, *5* (4), 546−562.

(5) Wen, H. P.; Deng, H.; Li, B. Y.; Chen, J. Y.; Zhu, J. Y.; Zhang, X.; Yoshida, S.; Zhou, Y. D. Mitochondrial diseases: From molecular mechanisms to therapeutic advances. *Signal Transduct. Target. Ther.* **2025**, *10* (1), 9.

(6) Vyas, S.; Zaganjor, E.; Haigis, M. C. Mitochondria and cancer. *Cell* **2016**, *166* (3), 555−566.

(7) Klemmensen, M. M.; Borrowman, S. H.; Pearce, C.; Pyles, B.; Chandra, B. Mitochondrial dysfunction in neurodegenerative disorders. *Neurotherapeutics* **2024**, *21* (1), No. e00292.

(8) Zong, Y.; Li, H.; Liao, P.; Chen, L.; Pan, Y.; Zheng, Y. Q.; Zhang, C. Q.; Liu, D. L.; Zheng, M. H.; Gao, J. J. Mitochondrial dysfunction: Mechanisms and advances in therapy. *Signal Transduct. Target. Ther.* **2024**, *9* (1), 124.

(9) Murphy, M. P.; Hartley, R. C. Mitochondria as a therapeutic target for common pathologies. *Nat. Rev. Drug Discovery* **2018**, *17* (12), 865−886.

(10) Picard, M.; Wallace, D. C.; Burelle, Y. The rise of mitochondria in medicine. *Mitochondrion* **2016**, *30*, 105−116.

(11) Giacomello, M.; Pyakurel, A.; Glytsou, C.; Scorrano, L. The cell biology of mitochondrial membrane dynamics. *Nat. Rev. Mol. Cell Biol.* **2020**, *21* (4), 204−224.

(12) Tábara, L. C.; Segawa, M.; Prudent, J. Molecular mechanisms of mitochondrial dynamics. *Nat. Rev. Mol. Cell Biol.* **2025**, *26* (2), 123−146.

(13) Liew, S. S.; Qin, X. F.; Zhou, J.; Li, L.; Huang, W.; Yao, S. Q. Smart design of nanomaterials for mitochondria-targeted nanotherapeutics. *Angew. Chem., Int. Ed.* **2021**, *60* (5), 2232−2256.

(14) Zielonka, J.; Joseph, J.; Sikora, A.; Hardy, M.; Ouari, O.; Vasquez-Vivar, J.; Cheng, G.; Lopez, M.; Kalyanaraman, B. Mitochondria-targeted triphenylphosphonium-based compounds: Syntheses, mechanisms of action, and therapeutic and diagnostic applications. *Chem. Rev.* **2017**, *117* (15), 10043−10120.
(15) Liu, J.; Cabral, H.; Mi, P. Nanocarriers address intracellular barriers for efficient drug delivery, overcoming drug resistance, subcellular targeting and controlled release. *Adv. Drug Delivery Rev.* **2024**, *207*, No. 115239.
(16) Pei, D. H.; Buyanova, M. Overcoming endosomal entrapment in drug delivery. *Bioconjugate Chem.* **2019**, *30* (2), 273−283.
(17) Nakamura, T.; Sato, Y.; Yamada, Y.; Abd Elwakil, M. M.; Kimura, S.; Younis, M. A.; Harashima, H. Extrahepatic targeting of lipid nanoparticles in vivo with intracellular targeting for future nanomedicines. *Adv. Drug Delivery Rev.* **2022**, *188*, No. 114417.
(18) Ng, M. Y. W.; Wai, T.; Simonsen, A. Quality control of the mitochondrion. *Dev. Cell* **2021**, *56* (7), 881−905.
(19) Omura, T. Mitochondria-targeting sequence, a multi-role sorting sequence recognized at all steps of protein import into mitochondria. *J. Biochem.* **1998**, *123* (6), 1010−1016.
(20) Muratovska, A.; Lightowlers, R. N.; Taylor, R. W.; Wilce, J. A.; Murphy, M. P. Targeting large molecules to mitochondria. *Adv. Drug Delivery Rev.* **2001**, *49* (1−2), 189−198.
(21) van der Bliek, A. M.; Shen, Q. F.; Kawajiri, S. Mechanisms of mitochondrial fission and fusion. *Cold Spring Harbor Perspect. Biol.* **2013**, *5* (6), No. a011072.
(22) Gao, S.; Hu, J. J. Mitochondrial fusion: The machineries in and out. *Trends Cell Biol.* **2021**, *31* (1), 62−74.
(23) Song, Z. Y.; Ghochani, M.; McCaffery, J. M.; Frey, T. G.; Chan, D. C. Mitofusins and OPA1 mediate sequential steps in mitochondrial membrane fusion. *Mol. Biol. Cell* **2009**, *20* (15), 3525−3532.
(24) von der Malsburg, A.; Sapp, G. M.; Zuccaro, K. E.; von Appen, A.; Moss, F. R.; Kalia, R.; Bennett, J. A.; Abriata, L. A.; Dal Peraro, M.; van der Laan, M.; Frost, A.; Aydin, H. Structural mechanism of mitochondrial membrane remodelling by human OPA1. *Nature* **2023**, *620* (7976), 1101−1108.
(25) de Brito, O. M.; Scorrano, L. Mitofusin 2 tethers endoplasmic reticulum to mitochondria. *Nature* **2008**, *456* (7222), 605−647.
(26) Al Amir Dache, Z.; Thierry, A. R. Mitochondria-derived cell-to-cell communication. *Cell Rep.* **2023**, *42* (7), No. 112728.
(27) König, T.; McBride, H. M. Mitochondrial-derived vesicles in metabolism, disease, and aging. *Cell Metab.* **2024**, *36* (1), 21−35.
(28) Crewe, C.; Funcke, J. B.; Li, S. J.; Joffin, N.; Gliniak, C. M.; Ghaben, A. L.; An, Y. A.; Sadek, H. A.; Gordillo, R.; Akgul, Y.; et al. Extracellular vesicle-based interorgan transport of mitochondria from energetically stressed adipocytes. *Cell Metab.* **2021**, *33* (9), 1853−1868.
(29) Kalluri, R.; LeBleu, V. S. The biology, function, and biomedical applications of exosomes. *Science* **2020**, *367* (6478), eaau6977.
(30) Gurung, S.; Perocheau, D.; Touramanidou, L.; Baruteau, J. The exosome journey: From biogenesis to uptake and intracellular signalling. *Cell Commun. Signaling* **2021**, *19* (1), 47.
(31) Alvarez-Erviti, L.; Seow, Y. Q.; Yin, H. F.; Betts, C.; Lakhal, S.; Wood, M. J. A. Delivery of siRNA to the mouse brain by systemic injection of targeted exosomes. *Nat. Biotechnol.* **2011**, *29* (4), 341−U179.
(32) Das, C. K.; Jena, B. C.; Banerjee, I.; Das, S.; Parekh, A.; Bhutia, S. K.; Mandal, M. Exosome as a novel shuttle for delivery of therapeutics across biological barriers. *Mol. Pharmaceutics* **2019**, *16* (1), 24−40.
(33) Wan, T.; Zhong, J. F.; Pan, Q.; Zhou, T. H.; Ping, Y.; Liu, X. R. Exosome-mediated delivery of Cas9 ribonucleoprotein complexes for tissue-specific gene therapy of liver diseases. *Sci. Adv.* **2022**, *8* (37), eabp9435 DOI: 10.1126/sciadv.abp9435.
(34) Li, Z.; Zhou, X.; Wei, M.; Gao, X.; Zhao, L.; Shi, R.; Sun, W.; Duan, Y.; Yang, G.; Yuan, L. In vitro and in vivo RNA inhibition by CD9-HuR functionalized exosomes encapsulated with miRNA or CRISPR/dCas9. *Nano Lett.* **2019**, *19* (1), 19−28.
(35) Joshi, B. S.; de Beer, M. A.; Giepmans, B. G.; Zuhorn, I. S. Endocytosis of extracellular vesicles and release of their cargo from endosomes. *ACS Nano* **2020**, *14* (4), 4444−4455.
(36) Heusermann, W.; Hean, J.; Trojer, D.; Steib, E.; von Bueren, S.; Graff-Meyer, A.; Genoud, C.; Martin, K.; Pizzato, N.; Voshol, J.; et al. Exosomes surf on filopodia to enter cells at endocytic hot spots, traffic within endosomes, and are targeted to the ER. *J. Biochem. Cell Biol.* **2016**, *213* (2), 173−184.
(37) Yang, J. L.; Zhang, X. F.; Chen, X. J.; Wang, L.; Yang, G. D. Exosome mediated delivery of miR-124 promotes neurogenesis after Ischemia. *Mol. Ther. Nucleic Acids* **2017**, *7*, 278−287.
(38) Kimiz-Gebologlu, I.; Oncel, S. S. Exosomes: Large-scale production, isolation, drug loading efficiency, and biodistribution and uptake. *J. Controlled Release* **2022**, *347*, 533−543.
(39) Tian, Y.; Xue, C.; Zhang, W.; Chen, C.; Ma, L.; Niu, Q.; Wu, L.; Yan, X. Refractive index determination of individual viruses and small extracellular vesicles in aqueous media using nano-flow cytometry. *Anal. Chem.* **2022**, *94* (41), 14299−14307.
(40) Gao, K. X.; Cheng, M.; Zuo, X. X.; Lin, J. Z.; Hoogewijs, K.; Murphy, M. P.; Fu, X. D.; Zhang, X. R. Active RNA interference in mitochondria. *Cell Res.* **2021**, *31* (2), 219−228.
(41) Kiss, T.; Filipowicz, W. Evidence against a mitochondrial location of the 7−2/MRP RNA in mammalian cells. *Cell* **1992**, *70* (1), 11−16.
(42) Gammage, P. A.; Moraes, C. T.; Minczuk, M. Mitochondrial genome engineering: The revolution may not be CRISPR-Ized. *Trends Genet.* **2018**, *34* (2), 101−110.
(43) Falkenberg, M.; Hirano, M. Editing the mitochondrial genome. *N. Engl. J. Med.* **2020**, *383* (15), 1489−1491.
(44) Peeva, V.; Blei, D.; Trombly, G.; Corsi, S.; Szukszto, M. J.; Rebelo-Guiomar, P.; Gammage, P. A.; Kudin, A. P.; Becker, C.; Altmüller, J. Linear mitochondrial DNA is rapidly degraded by components of the replication machinery. *Nat. Commun.* **2018**, *9* (11), 1727 DOI: 10.1038/s41467-018-04131-w.
(45) Fontana, G. A.; Gahlon, H. L. Mechanisms of replication and repair in mitochondrial DNA deletion formation. *Nucleic acids Res.* **2020**, *48* (20), 11244−11258.
(46) Nissanka, N.; Bacman, S. R.; Plastini, M. J.; Moraes, C. T. The mitochondrial DNA polymerase gamma degrades linear DNA fragments precluding the formation of deletions. *Nat. Commun.* **2018**, *9* (1), 2491.
(47) Wang, D. L.; Wang, J. N.; Bonamy, G. M. C.; Meeusen, S.; Brusch, R. G.; Turk, C.; Yang, P. Y.; Schultz, P. G. A small molecule promotes mitochondrial fusion in mammalian cells. *Angew. Chem., Int. Ed.* **2012**, *51* (37), 9302−9305.
(48) Zacharioudakis, E.; Agianian, B.; Kumar MV, V.; Biris, N.; Garner, T. P.; Rabinovich-Nikitin, I.; Ouchida, A. T.; Margulets, V.; Nordstrøm, L. U.; Riley, J. S.; Dolgalev, I.; Chen, Y.; Wittig, A. J. H.; Pekson, R.; Mathew, C.; Wei, P.; Tsirigos, A.; Tait, S. W. G.; Kirshenbaum, L. A.; Kitsis, R. N.; Gavathiotis, E. Modulating mitofusins to control mitochondrial function and signaling. *Nat. Commun.* **2022**, *13* (1), 3775.
(49) Herkenne, S.; Ek, O.; Zamberlan, M.; Pellattiero, A.; Chergova, M.; Chivite, I.; Novotná, E.; Rigoni, G.; Fonseca, T. B.; Samardzic, D.; et al. Developmental and tumor angiogenesis requires the mitochondria-shaping protein opa1. *Cell Metab.* **2020**, *31* (5), 987−1003.

https://doi.org/10.1021/acs.nanolett.6c00233
Nano Lett. 2026, 26, 6324−6333